



Effect of $\text{Li}_4\text{Ti}_5\text{O}_{12}$ Nanoparticles on Structural, Optical and Thermal Properties of PVDF/PEO Blend

F. H. Abd El-kader¹ · N. A. Hakeem² · R. S. Hafez¹ · A. M. Ismail²

Received: 22 October 2017 / Accepted: 4 December 2017 / Published online: 8 December 2017
© Springer Science+Business Media, LLC, part of Springer Nature 2017

Abstract

Lithium titanate nanoparticles $\text{Li}_4\text{Ti}_5\text{O}_{12}$ NPs were prepared by the solid-state reaction method using a stoichiometric ratio of lithium carbonate Li_2CO_3 and titanium oxide nanoparticles TiO_2 NPs. X-ray diffraction (XRD) analysis confirmed the formation of $\text{Li}_4\text{Ti}_5\text{O}_{12}$ NPs. High-resolution transmission electron microscope showed like—cube shape of $\text{Li}_4\text{Ti}_5\text{O}_{12}$ NPs with an average particle size 42 nm. Poly(vinylidene fluoride) (PVDF) and poly(ethylene oxide) (PEO) (80/20 wt/wt%) blend doped with concentrations 0.5, 0.7, 1.0, 2.0, 5.0 and 7.0 wt% of $\text{Li}_4\text{Ti}_5\text{O}_{12}$ NPs were prepared using casting technique. Structural, optical and thermal properties of polymer nanocomposites were investigated using XRD, high-resolution scanning electron microscope (HRSEM), energy dispersive spectrophotometer (EDS), Fourier transform infrared (FT-IR), ultraviolet–visible spectroscopy (UV–Vis) and differential scanning calorimetry (DSC). The XRD and FT-IR data showed that there was an interaction between the blend sample and $\text{Li}_4\text{Ti}_5\text{O}_{12}$ NPs. Also, the addition of $\text{Li}_4\text{Ti}_5\text{O}_{12}$ NPs decreased the degree of crystallinity of the blend sample. HRSEM images revealed that the presence of $\text{Li}_4\text{Ti}_5\text{O}_{12}$ NPs changed the surface morphology of the nanocomposites and gave rise to crystalline domains up to 5 wt% $\text{Li}_4\text{Ti}_5\text{O}_{12}$ NPs, then deteriorations was occurred.

Keywords $\text{Li}_4\text{Ti}_5\text{O}_{12}$ nanoparticles · XRD · HRTEM · FT-IR · DSC

1 Introduction

Polymer blending is one of the most important methods to build up new polymeric materials. In fact, it is a valuable and an easy method for designing materials with different physical properties [1–5]. Poly(vinylidene fluoride) (PVDF) is a semicrystalline polymer with repeating unit ($\text{CH}_2\text{—CF}_2$). It has high importance in the scientific and technological research due to its unique electrical, pyroelectric, ferroelectric and piezoelectric properties [6]. PVDF has various applications because it has good mechanical strength, stability against vigorous chemicals, good thermal stability and exceptional biocompatibility contrasted with other polymeric materials [7–9]. Poly(ethylene oxide) (PEO) is a semicrystalline polymer which has high chemical, thermal and electrochemical stability [10–12]. It can be used as a long

fiber dispersing agent in the manufacture of paper and adhesives, as a friction reduction, flocculating or thickening agent as lubricants and possesses a variety of further applications [13]. PEO is a simple chain polymer with etheric linkages. The C–O bond in the linkages will be one of the least reactive and sensitive bonds [14]. Both of the PVDF and PEO are soluble and miscible in dimethyl sulfoxide (DMSO). So blending PEO with PVDF may reduce its crystallinity and increase its ionic conductivity. The interaction between C–O–C group of PEO and CF_2 group of PVDF makes these two polymers to be compatible with each other [15]. Many researchers reported that (80/20 wt/wt%) of PVDF/PEO is the best ratio for compatibility and miscibility between PVDF and PEO homopolymers [16–20].

Metal nanoparticles combined with polymers are greatly attractive because of the various applications offered by these materials [21–24]. More development of the nanocomposites properties can be enhanced by loading nanofiller materials with aspect ratio [25]. $\text{Li}_4\text{Ti}_5\text{O}_{12}$ has spinel structure which is applied to the negative electrode in the lithium ion secondary battery. The properties of $\text{Li}_4\text{Ti}_5\text{O}_{12}$ are hardly expanded by the overcharge and high stability in cycles of discharging and charging [26, 27].

✉ R. S. Hafez
rsaber@sci.cu.edu.eg

¹ Physics Department, Faculty of Science, Cairo University, Giza 12613, Egypt

² Physics Division, Spectroscopy Department, National Research Centre, Giza 12622, Egypt

The present work aims to prepare $\text{Li}_4\text{Ti}_5\text{O}_{12}$ NPs via solid-state reaction method using Li_2CO_3 and rutile TiO_2 . Rutile TiO_2 was more desirable in acquiring high purity $\text{Li}_4\text{Ti}_5\text{O}_{12}$ than anatase due to the anatase to rutile phase transformation, which was found to be more rigid in the solid-state reaction than the intact rutile phase [28]. Nanocomposite films of (80/20 wt/wt%) PVDF/PEO doped with different concentrations of $\text{Li}_4\text{Ti}_5\text{O}_{12}$ NPs were prepared to study the effect of $\text{Li}_4\text{Ti}_5\text{O}_{12}$ NPs as filler on the structural, thermal and optical properties of PVDF/PEO blend by using suitable techniques.

2 Experimental Work

2.1 Preparation of $\text{Li}_4\text{Ti}_5\text{O}_{12}$ Nanoparticles

Ten millilitre of titanium tetrachloride (TiCl_4 , 98% purity, Fluka) was slowly added to 100 ml distilled water in an ice cool bath (due to the reaction is exothermic). The beaker was taken from ice bath to room temperature and kept in a magnetic stirrer to make homogenous solution at 100 °C till forming white precipitate. The obtained precipitate was dried at 100 °C for 12 h. For further phase transformation, it was calcined at 500 °C for about 3 h to obtain TiO_2 nanoparticles.

0.4 gm of prepared TiO_2 and 0.147 gm of Lithium carbonate (Li_2CO_3 , $M_w \approx 73.89$, 99% purity, Aldrich) were mixed in ceramic mortar for about 15 min. Then add drops of distilled water to the mixture to create slurry. The mixed slurry was dried at 60 °C and calcined for 5 h at 800 °C to obtain the final $\text{Li}_4\text{Ti}_5\text{O}_{12}$ nanoparticles.

2.2 Preparation of PVDF/PEO/ $\text{Li}_4\text{Ti}_5\text{O}_{12}$ Nanocomposite Films

Both PVDF ($M_w \approx 543.000$, Aldrich) and PEO [$M_w \approx 600.000$, ACROS] powders were dried at 60 °C in a vacuum oven about 1 h to remove any moisture. (80/20 wt/wt%) PVDF/PEO was dissolved in dimethyl sulfoxide (DMSO) then the polymer blend solution was stirred continuously until homogeneous viscous liquid was formed. $\text{Li}_4\text{Ti}_5\text{O}_{12}$ NPs were also suspended in DMSO using sonicator about 30 min. $\text{Li}_4\text{Ti}_5\text{O}_{12}$ NPs solution with mass fractions 0.5, 0.7, 1.0, 2.0, 5.0 and 7.0 wt% was added drop by drop to the polymer blend solution. For a good dispersion, the resulting solution was sonicated to approach homogeneity and good wet ability. Then the solution was cast onto Petri dishes and kept in a vacuum oven at 70 °C about 12 h until the solvent completely evaporated. After drying, the films were peeled from Petri dishes and kept in a vacuum desiccator until uses.

2.3 Measurement Techniques

The X-ray diffraction (XRD) was performed using PANalytical X'Pert Pro target Cu-K α with secondary monochromator Holland radiation ($\lambda = 0.1540$ nm, the tube operated at 45 kV, scans were collected over a 2θ range of 5°–60°). High-resolution scanning electron microscope (HRSEM) with EDX detector was performed using SEM Model Quanta 250 FEG. High-resolution transmission electron microscope (HRTEM) was performed by JEM-2100F electron microscope with accelerating voltage of 200 kV. Fourier transform infrared (FT-IR) measurements were taken using JASCO, FT/IR-6100 in the spectral range of 4000–400 cm^{-1} . Ultraviolet–visible absorption spectra (UV–Vis) were measured in the wave length region of 200–800 nm using UV-630 (Shimadzu) UV–VIS–NIR spectrophotometer. Differential scanning calorimetry (DSC) of the prepared samples was carried out using (DSC-50, Shimadzu, Japan) with measuring temperature range from room temperature to 200 °C and the heating rate was 10 °C/min.

3 Results and Discussion

3.1 X-Ray Diffraction (XRD)

Figure 1a shows the XRD pattern of TiO_2 NPs. It shows diffraction peaks at 2θ values of 27.3°, 36.2°, 39.1°, 41.2°, 44.0°, 54.2° and 56.5°. These peaks correspond to (110), (101), (200), (111), (210), (211) and (220) planes respectively. All the diffraction peaks matched well with the tetragonal rutile TiO_2 according to the standard pattern (JCPDS card No. 01-089-0552).

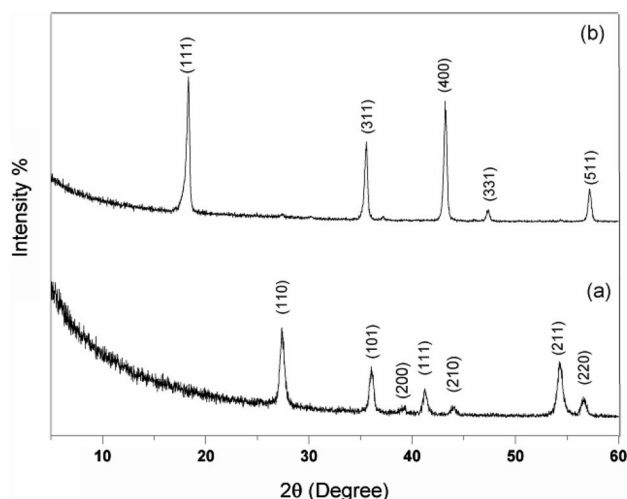


Fig. 1 XRD patterns of (a) TiO_2 and (b) $\text{Li}_4\text{Ti}_5\text{O}_{12}$ nanoparticles

The half-width of peaks is related to the crystallite dimensions. The average particle size was estimated from the Scherrer equation on the rutile phase diffraction peaks (the most intense peaks) [9].

$$D = \frac{K\lambda}{\beta \cos \theta} \quad (1)$$

where D is the crystal size, λ is the X-ray wavelength, β is the full width at half maximum (FWHM) of the diffraction peak (radian), K is a constant (0.89) and θ is the diffraction angle at the peak maximum. The calculated average crystal size of rutile TiO_2 NPs was found to be around 20 nm.

Figure 1b shows the XRD pattern of $\text{Li}_4\text{Ti}_5\text{O}_{12}$ NPs. All diffraction peaks matched with standard $\text{Li}_4\text{Ti}_5\text{O}_{12}$ (JCPDS Card No. 01-072-0427). The sharp and well resolved peaks obtained at 2θ values of 18.3° , 35.6° , 43.2° , 47.3° and 57.2° indicate the high crystalline nature of $\text{Li}_4\text{Ti}_5\text{O}_{12}$ NPs. These diffraction peaks correspond to (111), (311), (400), (331) and (511) planes of cubic spinel $\text{Li}_4\text{Ti}_5\text{O}_{12}$ NPs, respectively. The calculated average crystal size of $\text{Li}_4\text{Ti}_5\text{O}_{12}$ NPs according to Scherrer equation was found to be around 36.7 nm.

Figure 2 shows the XRD patterns of PVDF and PEO homopolymers at room temperature. Pure PVDF has diffraction peaks at 2θ values of 18.1° , 20.2° , 36.1° and 39.3° . These peaks correspond to (020), (110), (200) and (002) planes respectively [29–31]. While pure PEO has diffraction peaks at 2θ values of 19.1° , 23.3° , 26.5° , 27.2° and 39.9° which correspond to (120), (112), (222), (111) and (118) planes respectively [32, 33]. The XRD patterns indicate the semicrystalline structure of PVDF and PEO homopolymers.

Figure 3 represents the XRD patterns of PVDF/PEO blend films undoped and doped with different concentrations of $\text{Li}_4\text{Ti}_5\text{O}_{12}$ NPs in the scanning range $5^\circ \leq 2\theta \leq 60^\circ$. Spectrum (3a), for undoped blend sample, shows well defined

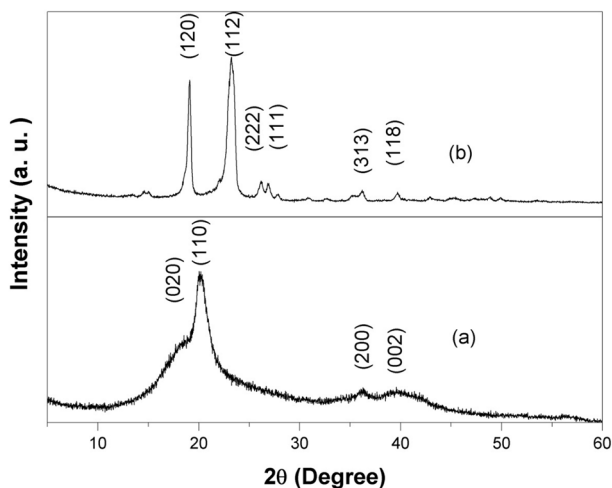


Fig. 2 XRD patterns of (a) PVDF and (b) PEO homopolymers

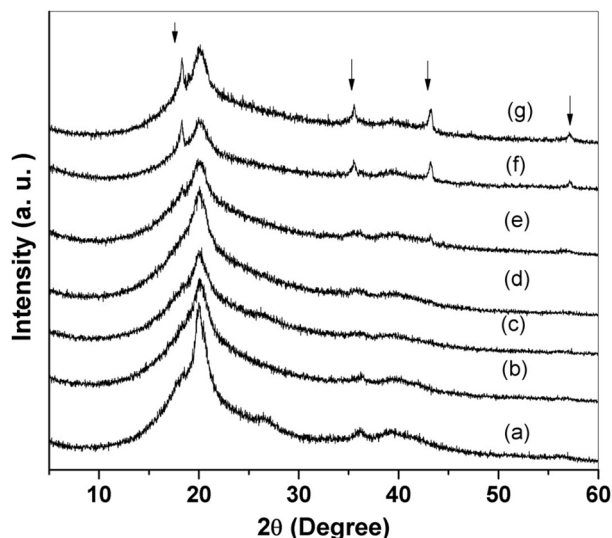


Fig. 3 XRD patterns of PVDF/PEO blend sample doped with: (a) 0.0, (b) 0.5, (c) 0.7, (d) 1.0, (e) 2.0, (f) 5.0 and (g) 7.0 wt% of $\text{Li}_4\text{Ti}_5\text{O}_{12}$ nanoparticles (the inside arrows clarify the undissociated of $\text{Li}_4\text{Ti}_5\text{O}_{12}$ nanoparticles)

diffraction peaks at 2θ values of 20.2° , 26.6° , 36.1° and 39.3° . The characteristic diffraction peaks of pure PEO were disappeared in undoped blend sample, which means that PEO incorporates into PVDF indicating the homogeneity between PVDF and PEO. However, the peak at $2\theta = 20.2^\circ$ is related to PVDF, suggesting that the semicrystalline nature of PVDF is still kept up in the blend. The spectra (3b–3g) show XRD patterns of blend sample doped with different concentrations of $\text{Li}_4\text{Ti}_5\text{O}_{12}$ NPs. The intensity of the peak at $2\theta = 20.2^\circ$ decreases randomly with various concentrations of $\text{Li}_4\text{Ti}_5\text{O}_{12}$ NPs. Also, the peak broadening slightly increases with increasing $\text{Li}_4\text{Ti}_5\text{O}_{12}$ NPs concentrations with respect to the undoped blend sample. These results confirm that the addition of $\text{Li}_4\text{Ti}_5\text{O}_{12}$ NPs decreases the degree of crystallinity of the blend sample. Contribution to the broadening can be due to lattice distortion, structural disorder as well as instrumental effects. On the other hand, all peaks of $\text{Li}_4\text{Ti}_5\text{O}_{12}$ NPs disappeared in doped samples with $\text{Li}_4\text{Ti}_5\text{O}_{12}$ NPs content ≤ 1.0 wt%. This shows the complete dissolution of nanoparticles in amorphous regions of the polymer blend. It is noticed that the diffraction peaks at $2\theta = 18.3^\circ$, 35.6° , 43.2° and 57.2° that appeared at concentrations ≥ 2.0 wt% $\text{Li}_4\text{Ti}_5\text{O}_{12}$ are assigned to $\text{Li}_4\text{Ti}_5\text{O}_{12}$ NPs. Also, their intensities increase with increasing $\text{Li}_4\text{Ti}_5\text{O}_{12}$ content in the blend sample.

3.2 Morphological Properties

Figure 4 shows HRSEM and HRTEM images of $\text{Li}_4\text{Ti}_5\text{O}_{12}$ NPs. The HRSEM image of $\text{Li}_4\text{Ti}_5\text{O}_{12}$ NPs exhibits uniform

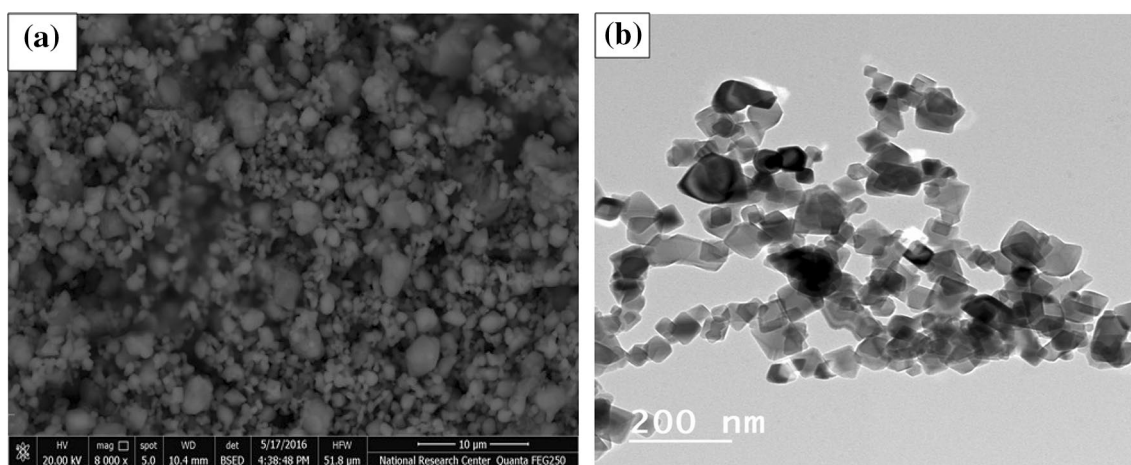


Fig. 4 **a** HRSEM and **b** HRTEM images of $\text{Li}_4\text{Ti}_5\text{O}_{12}$ nanoparticles

particle distribution with different particle sizes, while HRTEM image of $\text{Li}_4\text{Ti}_5\text{O}_{12}$ NPs shows a nearly cubic shape with average particle size in nanometer scale (42 nm). This value is larger than that obtained from XRD results because XRD gives the crystallite size whereas TEM gives the particle size that may consist of more than one crystallite.

Figure 5 shows HRSEM images of PVDF/PEO blend undoped and doped with different concentrations of $\text{Li}_4\text{Ti}_5\text{O}_{12}$ NPs. HRSEM micrographs show the changes in the surface morphology. As seen in Fig. 5a the surface is smooth with some irregularly shaped clusters regarding to the nature of PEO. The distribution of $\text{Li}_4\text{Ti}_5\text{O}_{12}$ NPs inside the PVDF/PEO blend is seen in Fig. 5b–g. $\text{Li}_4\text{Ti}_5\text{O}_{12}$ NPs appeared as small white particles that dispersed on the surface of the blend with some agglomerations. $\text{Li}_4\text{Ti}_5\text{O}_{12}$ agglomerations increase with increasing $\text{Li}_4\text{Ti}_5\text{O}_{12}$ content and the blend surface appears as separated domains until concentration 5 wt% $\text{Li}_4\text{Ti}_5\text{O}_{12}$ NPs. Whereas at concentration 7 wt% $\text{Li}_4\text{Ti}_5\text{O}_{12}$ NPs the film is seen to be deteriorating. Figures 6 and 7 show the element mapping and corresponding EDS analysis of samples 0.5 and 2.0 wt% of $\text{Li}_4\text{Ti}_5\text{O}_{12}$ NPs. These figures confirm the well distribution of $\text{Li}_4\text{Ti}_5\text{O}_{12}$ NPs on the surface of PVDF/PEO blend sample.

3.3 Fourier Transform Infrared Analysis (FT-IR)

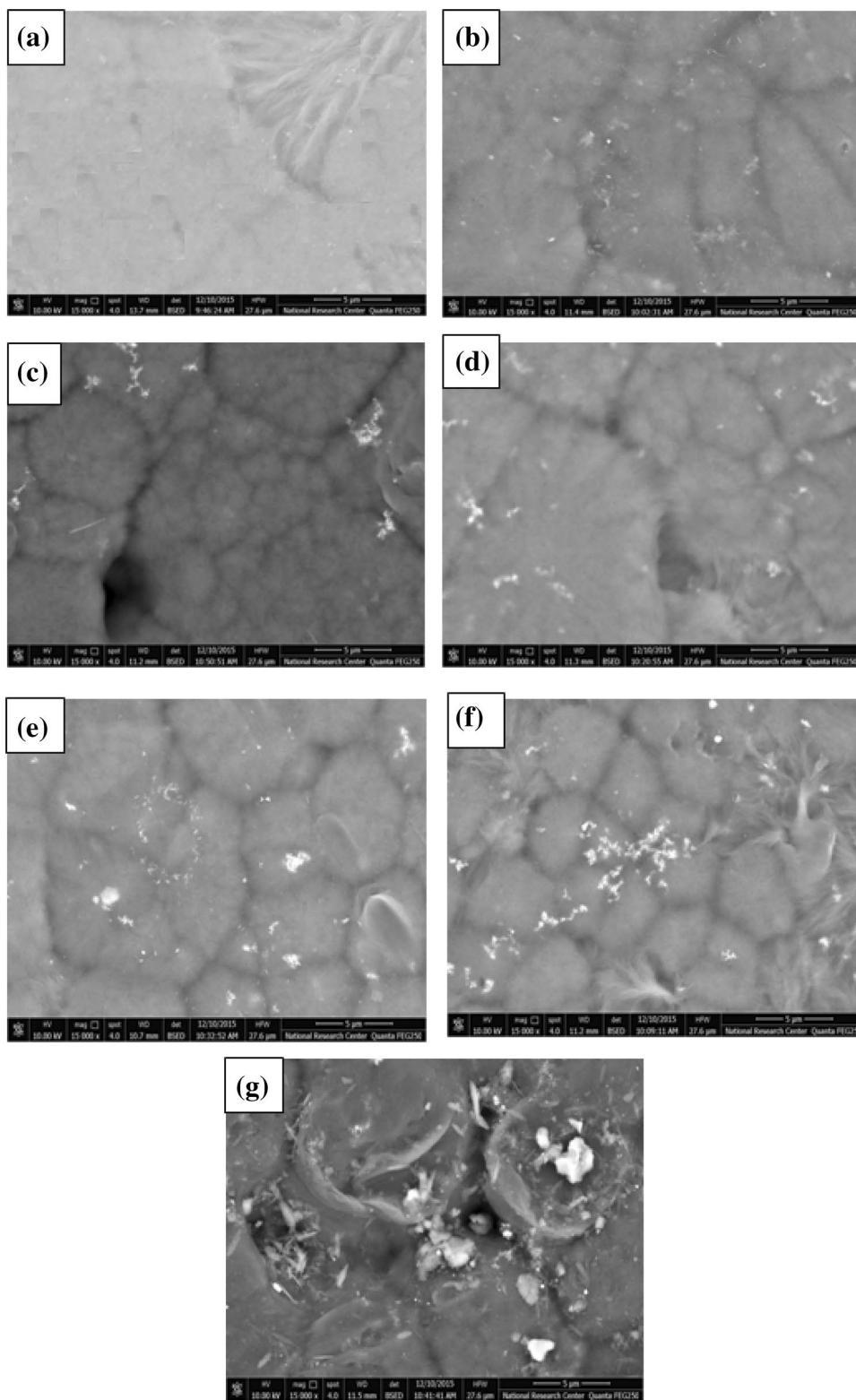
Figure 8 shows FT-IR spectra of TiO_2 NPs and $\text{Li}_4\text{Ti}_5\text{O}_{12}$ NPs were measured at room temperature from 4000 to 400 cm^{-1} . In both spectra, the bands at 3436 and 1631 cm^{-1} are attributed to O–H stretching and bending vibration mode for TiO_2 NPs and $\text{Li}_4\text{Ti}_5\text{O}_{12}$ NPs, respectively [34, 35]. The absorption bands at 523 and 645 cm^{-1} in TiO_2 NPs and $\text{Li}_4\text{Ti}_5\text{O}_{12}$ NPs respectively are attributed to Ti–O stretching vibration [36]. In $\text{Li}_4\text{Ti}_5\text{O}_{12}$ NPs spectrum, the band at 462 cm^{-1} is assigned to the Li–O vibration.

FT-IR spectra of PVDF, PEO homopolymers and PVDF/PEO blend sample are shown in Fig. 9. The position and the assignments of the vibrational bands of pure PVDF and PEO are organized in Table 1 which matched with previous results [6, 37–41]. The FT-IR spectrum of PVDF/PEO blend film shows a new peak at 1728 cm^{-1} which may be related to the interaction between the fluorine in PVDF and the carbon of PEO. The absorption bands at 1464 and 1342 cm^{-1} that corresponded to CH_2 scissoring and wagging mode in PEO homopolymer are disappeared. Also, the band at 1092 cm^{-1} is shifted to 1102 cm^{-1} . These changes in the blend spectrum compared to the individual polymers spectra confirm that there is an interaction between the PVDF and PEO homopolymers. Figure 10 represents the FT-IR spectra of PVDF/PEO blend films doped with different concentrations of $\text{Li}_4\text{Ti}_5\text{O}_{12}$ NPs. The absorption band at 1728 cm^{-1} becomes faint and the bands at 1102 cm^{-1} is shifted to 1110 cm^{-1} with adding $\text{Li}_4\text{Ti}_5\text{O}_{12}$ NPs. The FT-IR study declares the possibility of the interaction between the $\text{Li}_4\text{Ti}_5\text{O}_{12}$ NPs and the PVDF/PEO blend due to the changes in the fingerprint regions of FT-IR spectra. This result confirms what has been observed with XRD investigation.

3.4 Ultraviolet–Visible Spectroscopy (UV–Vis)

The UV–Vis spectra measurements were taken at room temperature in the range of 200–800 nm as shown in Fig. 11. The spectrum (11a) of undoped blend sample shows an intense band at 215 nm as a result of $\pi \rightarrow \pi^*$ electronic transition [42, 43]. This band attributed to the chromophoric groups of PVDF and PEO. The spectra (b–g) of the blend samples doped with various concentrations of $\text{Li}_4\text{Ti}_5\text{O}_{12}$ contain an additional band at 283 nm which attributed to $\text{Li}_4\text{Ti}_5\text{O}_{12}$ NPs. The intensity of the band at 215 nm increases with increasing $\text{Li}_4\text{Ti}_5\text{O}_{12}$ NPs

Fig. 5 HRSEM images of PVDF/PEO blend sample doped with: **a** 0.0, **b** 0.5, **c** 0.7, **d** 1.0, **e** 2.0, **f** 5.0 and **g** 7.0 wt% of $\text{Li}_4\text{Ti}_5\text{O}_{12}$ nanoparticles



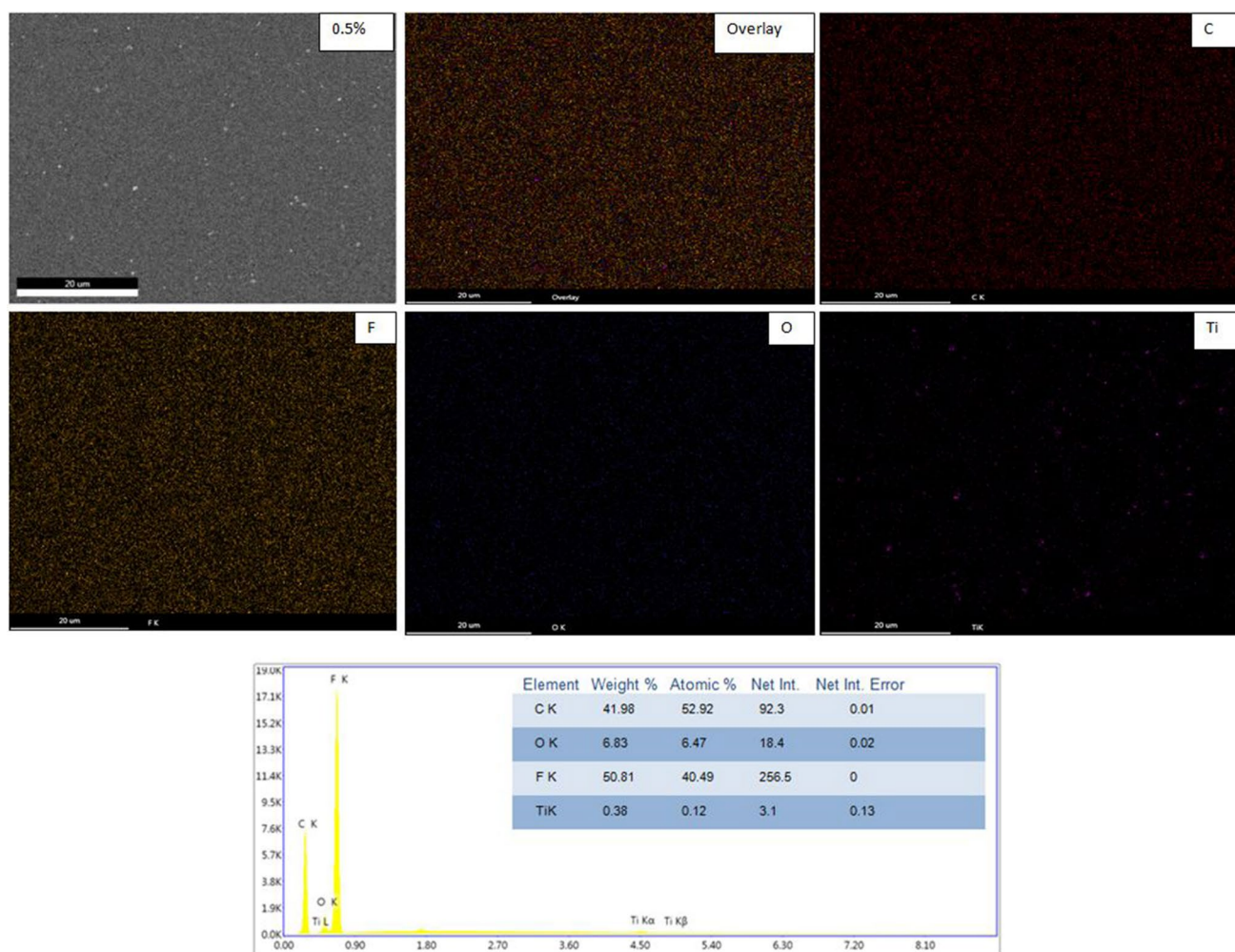


Fig. 6 HRSEM images and element mapping and corresponding EDS analysis of PVDF/PEO blend sample doped with 0.5 wt% of $\text{Li}_4\text{Ti}_5\text{O}_{12}$ nanoparticles

content up to 1.0 wt% then decreases after that. A new band appears at 242 nm at concentration 5.0 and 7.0 wt% of $\text{Li}_4\text{Ti}_5\text{O}_{12}$ which are due to the undissociated $\text{Li}_4\text{Ti}_5\text{O}_{12}$ NPs in the blend sample. These results confirmed that there is an interaction between the polymer blend and the nanofiller. For all samples, there are no absorption bands in the visible region because of the transparency of the prepared films.

The feature of the optical transition in the investigated films can be demonstrated by the dependence of the absorption coefficient (α) on the photon energy ($h\nu$). The absorption coefficient (α) is related to the absorbance (A) by the following relation [44]:

$$I = I_0 \exp(-\alpha d) \quad (2)$$

Hence;

$$\alpha = \frac{2.303}{d} \log \left(\frac{I_0}{I} \right) = \frac{2.303}{d} A \quad (3)$$

where I_0 and I are the intensities of the incident and the transmitted radiation respectively, d is the thickness of the sample.

Figure 12 shows the relation between α against $h\nu$ for PVDF/PEO blend films undoped and doped with different concentrations of $\text{Li}_4\text{Ti}_5\text{O}_{12}$ NPs. The extrapolations of the linear portion of the curves with x-axis are used to estimate the values of the absorption edge which are tabulated in Table 2. It is clear that the values of the absorption edge for doped PVDF/PEO films decreased with increasing $\text{Li}_4\text{Ti}_5\text{O}_{12}$ content. So, the degree of crystallinity of the blend sample decreases by doping with $\text{Li}_4\text{Ti}_5\text{O}_{12}$ NPs. This attributed to the change in the number of final states and/or the formation of localized states within the band gap because of the compositional disorder.

The values of α for all samples are relatively small indicating the weakly absorbing of the materials. In the exponent edge where ($1 < \alpha < 10^4$) α is restricted by an empirical relation due to Urbach [45].

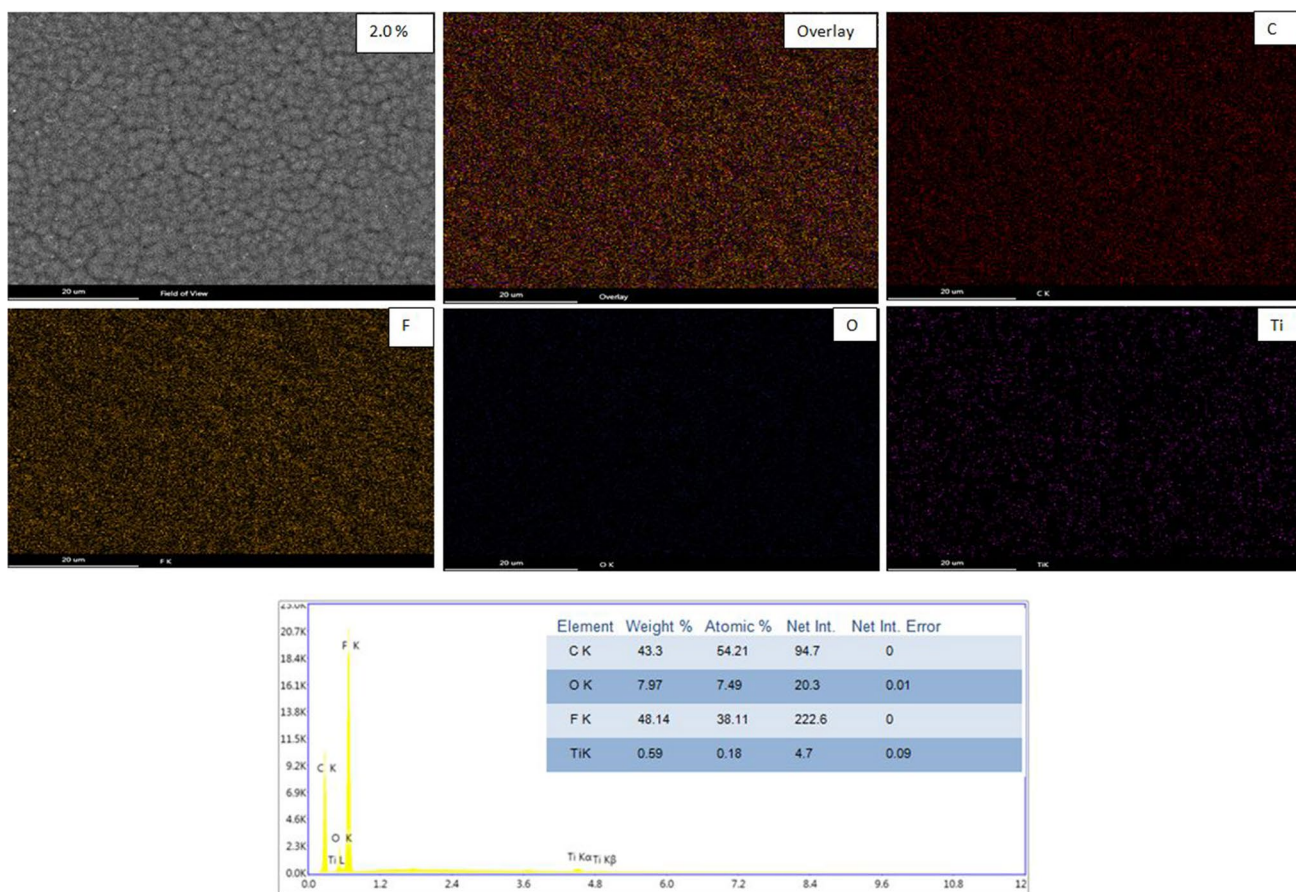


Fig. 7 HRSEM images and element mapping and corresponding EDS analysis of PVDF/PEO blend sample doped with 2.0 wt% of $\text{Li}_4\text{Ti}_5\text{O}_{12}$ nanoparticles

$$\alpha(\nu) = \alpha_0 \exp\left(\frac{h\nu}{E_e}\right) \quad (4)$$

where α_0 is a constant and E_e is the width of the tail of the localized states in the band gap. The estimated values of the band tail E_e for the investigated samples were determined from the reciprocal of slopes of linear portions of the plot between $\ln \alpha$ versus $h\nu$ see Fig. 13. The values of E_e for all samples are recorded in Table 2. From the data, we can see that the band tail values increase with increasing the concentrations of $\text{Li}_4\text{Ti}_5\text{O}_{12}$ NPs in the blend system. This means that the cluster size of $\text{Li}_4\text{Ti}_5\text{O}_{12}$ NPs increase i.e. there is rise in atomic densities due to the bonding between $\text{Li}_4\text{Ti}_5\text{O}_{12}$ NPs and PVDF/PEO film. However, the formation of the dopant aggregates leads to increase the defect size and a modified band form could be considered.

For more precise we measured the reflectance (R) to compute the refractive index (n) for the different samples (see Fig. 14a), the refractive index can be determined by the following relation [23]:

$$n = (1 + R^{1/2}) / (1 - R^{1/2}) \quad (5)$$

Figure 14b shows the dependence of the refractive index on the wavelength in the range 400–800 nm for undoped and doped samples with different concentrations with $\text{Li}_4\text{Ti}_5\text{O}_{12}$ NPs. From the figure, we can see that the values of (n) decrease slowly with increasing wavelength. At long wavelengths the change becomes insignificant. The nearly constant values of the refractive index (n_0) at long wavelengths with $\text{Li}_4\text{Ti}_5\text{O}_{12}$ NPs content are listed in Table 2.

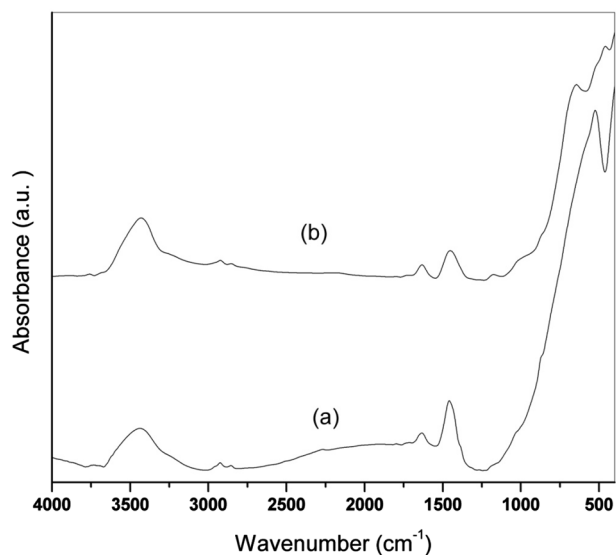


Fig. 8 FT-IR of (a) TiO_2 and (b) $\text{Li}_4\text{Ti}_5\text{O}_{12}$ nanoparticles

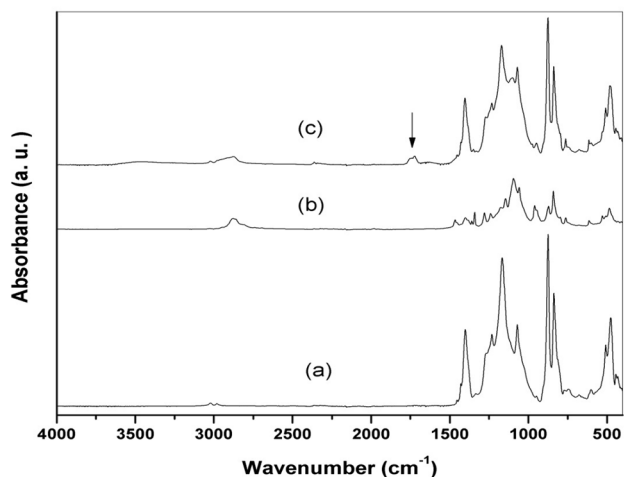


Fig. 9 FT-IR absorption spectra of (a) pure PVDF, (b) pure PEO and (c) PVDF/PEO blend (the inside arrow related to a new peak at 1728 cm^{-1})

The relatively high values of (n_0) of the samples may be related to the increasing in the valance density of charge carriers and increasing the scattering of the incident light [23]. The production of high refractive index in transparent

composite films is essential for the development of many photonic applications such as ultra-low loss optical waveguide and more efficient given for nonlinear devices.

3.5 Differential Scanning Calorimetry (DSC)

Figure 15 shows the DSC thermograms of PVDF and PEO homopolymers from room temperature to $200\text{ }^\circ\text{C}$. Only one endothermic peak was detected corresponding to the melting temperature of PVDF and PEO. The melting temperature T_m is found to be 157 and $69\text{ }^\circ\text{C}$ for PVDF and PEO homopolymers, respectively. Figure 16 shows the DSC thermograms of PVDF/PEO undoped blend sample and doped with different concentrations of $\text{Li}_4\text{Ti}_5\text{O}_{12}$ NPs. All samples show endothermic peak at $\sim 162\text{ }^\circ\text{C}$ which corresponds to the melting temperature of PVDF that is above the melting point of pure PVDF. Also, this endothermic peak is more broadening than that of the pure PVDF which indicating the reduction in crystallinity of nanocomposite samples. This indicates the compatibility between PVDF and PEO. The values of T_m for PVDF/PEO undoped blend sample and doped with different concentrations of $\text{Li}_4\text{Ti}_5\text{O}_{12}$ NPs are listed in Table 3. The data show that the melting temperature of the doped samples increases irregularly with respect to the undoped sample.

The degree of crystallinity (Δx) of PVDF is measured from the heat of fusion at melting for PVDF as the ratio between the heat of fusion of PVDF and the heat of fusion of 100% crystalline of pure PVDF ($\Delta H_{f(100)} = 104.6\text{ J g}^{-1}$) [46] by the following Eq. [47].

$$\Delta x = \frac{\Delta H_f}{\Delta H_{f(100)}} \times 100 \quad (6)$$

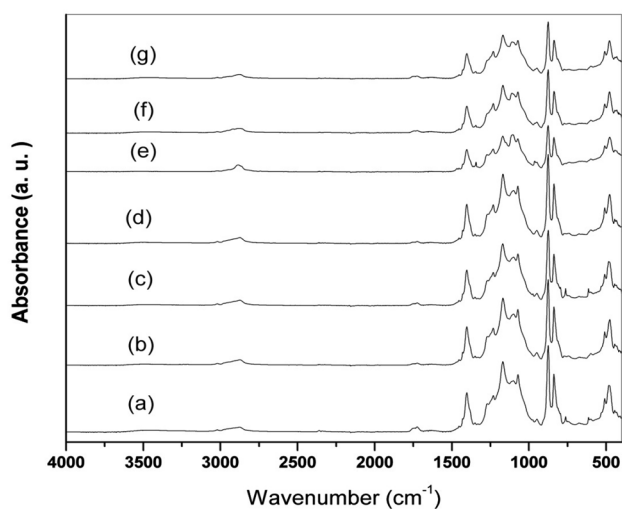
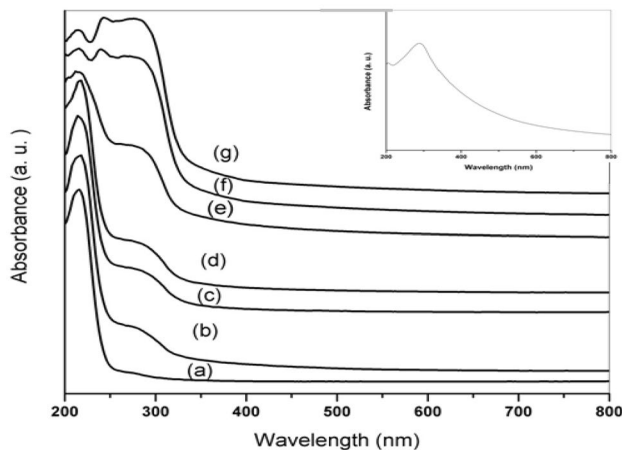
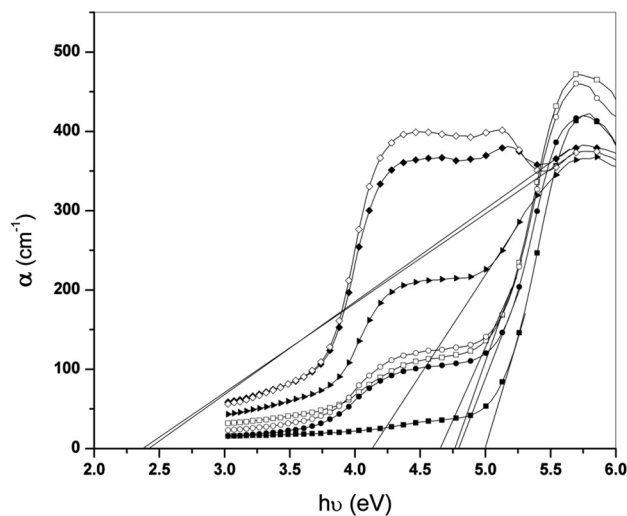
The degree of crystallinity values of PVDF after adding $\text{Li}_4\text{Ti}_5\text{O}_{12}$ NPs to the blend film are recorded in Table 3. It is clear that the values of degree of crystallinity change irregularly but still lower than that value of the undoped blend sample.

4 Conclusion

$\text{Li}_4\text{Ti}_5\text{O}_{12}$ NPs were prepared using the solid-state reaction method with an average particle size 42 nm and like cube shape. System of PVDF/PEO undoped blend sample and doped with different concentrations of $\text{Li}_4\text{Ti}_5\text{O}_{12}$ NPs was

Table 1 The assignments of most intense absorption bands for PVDF and PEO homopolymers

PVDF		PEO	
Wave number (cm ⁻¹)	Assignment	Wave number (cm ⁻¹)	Assignment
1404	CH ₂ wagging mode	2884	CH ₂ stretching mode
1237	CF out of plane	1464	CH ₂ scissoring mode
1167	CF ₂ asymmetric stretching mode	1342	CH ₂ wagging mode
1066	CH ₂ wagging	1246	CH ₂ twisting mode
880	C–C–C asymmetrical stretching vibration	1143 and 1092	C–O–C stretching mode
839	CH ₂ rocking	962	CH ₂ rocking and C–O–C vibration mode
478	CF ₂ bending mode	839	CH ₂ rocking
		528	C–O–C bending

**Fig. 10** FT-IR absorption spectra of PVDF/PEO blend sample doped with: (a) 0.0, (b) 0.5, (c) 0.7, (d) 1.0, (e) 2.0, (f) 5.0 and (g) 7.0 wt% of Li₄Ti₅O₁₂ nanoparticles**Fig. 11** UV-Vis spectra of PVDF/PEO blend sample doped with: (a) 0.0, (b) 0.5, (c) 0.7, (d) 1.0, (e) 2.0, (f) 5.0 and (g) 7.0 wt% of Li₄Ti₅O₁₂ nanoparticles**Fig. 12** Relation between absorbance coefficient (α) versus $h\nu$ for PVDF/PEO blend sample doped with: (filled square) 0.0 (open square) 0.5, (filled circle) 0.7, (open circle) 1.0, (filled right pointing triangle) 2.0, (filled diamond) 5.0 and (open diamond) 7.0 wt% of Li₄Ti₅O₁₂ nanoparticles**Table 2** The values of the absorption edge, band tail and refractive index (n_0) values for PVDF/PEO blend with different concentrations of Li₄Ti₅O₁₂ NPs

Li ₄ Ti ₅ O ₁₂ wt%	Absorption edge (eV)	Band tail (eV)	n_0
0.0	5.00	0.42	1.057
0.5	4.78	0.96	1.079
0.7	4.75	1.09	1.078
1.0	4.65	1.19	1.087
2.0	4.13	2.17	1.102
5.0	2.42	2.74	1.110
7.0	2.38	4.08	1.114

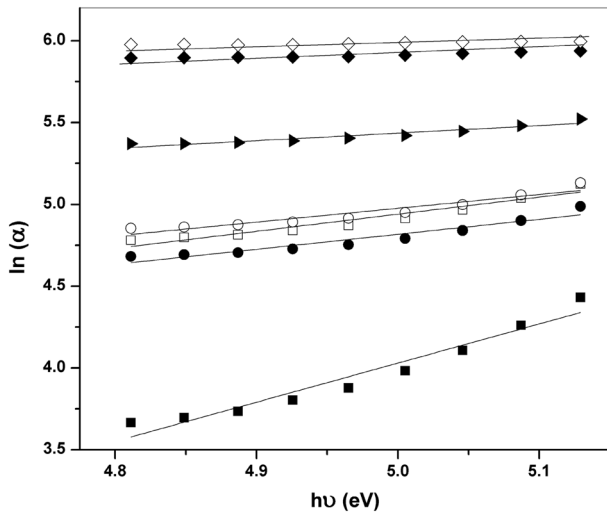


Fig. 13 Relation between $\ln(\alpha)$ versus $h\nu$ for PVDF/PEO blend sample doped with: (filled square) 0.0 (open square) 0.5, (filled circle) 0.7, (open circle) 1.0, (filled right pointing triangle) 2.0, (filled diamond) 5.0 and (open diamond) 7.0 wt% of $\text{Li}_4\text{Ti}_5\text{O}_{12}$ nanoparticles

prepared using casting technique method. The XRD and FT-IR data showed that there was an interaction between the blend sample and $\text{Li}_4\text{Ti}_5\text{O}_{12}$ NPs. The UV–Visible data revealed that the values of band tail increase with increasing the concentration of $\text{Li}_4\text{Ti}_5\text{O}_{12}$ NPs in blend sample. This confirmed the increase in the disorder in such

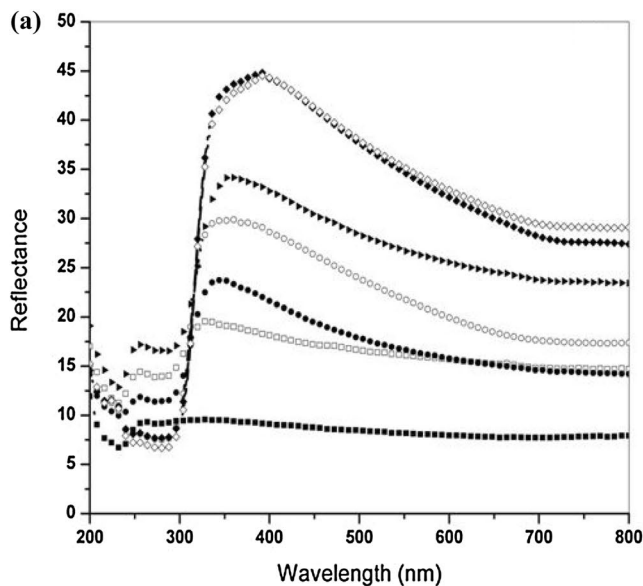


Fig. 14 Relation between **a** reflectance and **b** refractive index versus wavelength for PVDF/PEO blend sample doped with: (filled square) 0.0 (open square) 0.5, (filled circle) 0.7, (open circle) 1.0, (filled right

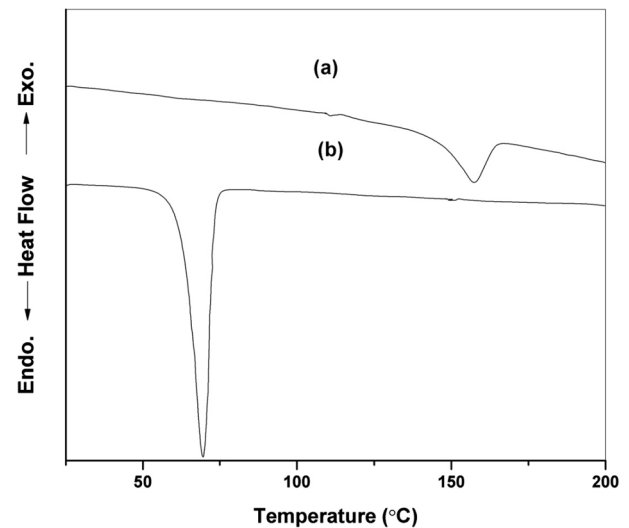
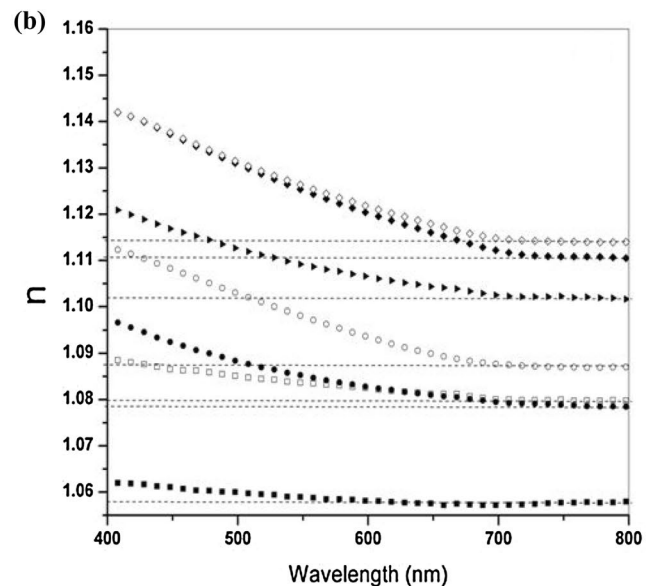


Fig. 15 DSC of (a) pure PVDF and (b) pure PEO homopolymers

system. The relatively high values of refractive index of the prepared samples were related to the increase in the valance density of the charge carriers and increase the scattering of the incident light. DSC revealed the reduction of the degree of crystallinity of the polyblend system. SEM and EDS mapping showed that $\text{Li}_4\text{Ti}_5\text{O}_{12}$ NPs



pointing triangle) 2.0, (filled diamond) 5.0 and (open diamond) 7.0 wt% of $\text{Li}_4\text{Ti}_5\text{O}_{12}$ nanoparticles

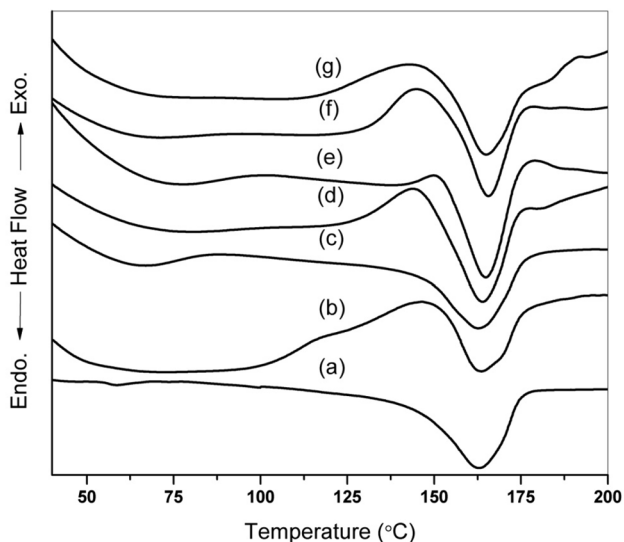


Fig. 16 DSC of PVDF/PEO blend sample doped with: (a) 0.0, (b) 0.5, (c) 0.7, (d) 1.0, (e) 2.0, (f) 5.0 and (g) 7.0 wt% of $\text{Li}_4\text{Ti}_5\text{O}_{12}$ nanoparticles

Table 3 The values of $T_{m(\text{PVDF})}$, $\Delta H_{f(\text{PVDF})}$ and $\Delta X_{(\text{PVDF})}$ for PVDF/PEO blend doped with different concentration of $\text{Li}_4\text{Ti}_5\text{O}_{12}$ NPs

$\text{Li}_4\text{Ti}_5\text{O}_{12}$ wt%	$T_{m(\text{PVDF})}$ (°C)	$\Delta H_{f(\text{PVDF})}$ (J g^{-1})	$\Delta X_{(\text{PVDF})}$ (%)
0.0	162.42	33.16	31.70
0.5	164.02	25.24	24.13
0.7	162.74	28.85	27.58
1.0	164.33	32.21	30.79
2.0	165.27	27.73	26.51
5.0	166.04	27.84	26.61
7.0	165.44	22.96	21.95

are well dispersed on the surface of the blend with some agglomerations. Also, the film surface appeared as separated domains until concentration 5 wt% $\text{Li}_4\text{Ti}_5\text{O}_{12}$ NPs. Whereas at concentration 7 wt% $\text{Li}_4\text{Ti}_5\text{O}_{12}$ NPs the film was seen to be deteriorating.

References

- A.G. Supri, M.D. SitiHajar, M.P.M. Hanif, Effect of type of conductive fillers and poly(ethylene glycol) diglycidyl ether on the electrical conductivity and morphology properties of poly(vinyl chloride)/poly(ethylene oxide) conductive films. *Polym. Bull.* **73**, 2831 (2016)
- O. Abdullah, D. Saber, L. Hamasalih, Complexion formation in PVA/PEO/ CuCl_2 solid polymer electrolyte. *Univers. J. Mater. Sci.* **3**, 1 (2015)
- K. Hemalatha, H. Somashekarappa, R. Somashekar, Preparation and characterization of MMT doped PVA/SA polymer composites. *Adv. Mater. Phys. Chem.* **4**, 172 (2014)
- N. Rajeswari, S. Selvasekarapandian, S. Karthikeyan, M. Prabu, G. Hirankumar, H. Nithya, C. Sanjeeviraja, Conductivity and dielectric properties of poly(vinyl alcohol)-poly(vinyl pyrrolidone) poly blend film using non-aqueous medium. *J. Non-Cryst. Solids* **357**, 3751 (2011)
- E.M. Abdelrazek, I.S. Elashmawi, A. El-khodary, A. Yassin, Structural, optical, thermal and electrical studies on PVA/PVP blends filled with lithium bromide. *Curr. Appl. Phys.* **10**, 607 (2010)
- D.S. Rana, D.K. Chaturvedi, J.K. Quamara, Morphology, crystalline structure, and chemical properties of 100 MeV Ag-ion beam irradiated poly(vinylidene fluoride) (PVDF) thin film. *J. Optoelectron. Adv. Mater.* **11**, 705 (2009)
- F. Liu, Y.-Y. Xu, B.-K. Zhua, F. Zhanga, L.-P. Zhu, Preparation of hydrophilic and fouling resistant poly(vinylidene fluoride) hollow fiber membranes. *J. Membr. Sci.* **345**, 331 (2009)
- F. Liu, N.A. Hashim, Y. Liu, M.R.M. Abed, K. Li, Progress in the production and modification of PVDF membranes. *J. Membr. Sci.* **375**, 1 (2011)
- S. Rajabzadeh, T. Maruyama, Y. Ohmukai, T. Sotani, H. Matsuyama, Preparation of PVDF/PMMA blend hollow fiber membrane via thermally induced phase separation (TIPS) method. *Sep. Purif. Technol.* **66**, 76 (2009)
- K.N. Kumar, B.H. Rudramadevi, S. Buddhudu, Energy transfer based photoluminescence spectra of Dy^{3+} , Sm^{3+} : PEO + PVP polymer films. *Indian J. Pure Appl. Phys.* **52**, 588 (2014)
- A.M. Abdelghany, M.S. Meikhail, N.A. Elsheshtawy, H.Y. Salah, Structural and thermal stabilization correlation of PEO/PVA-AgCl polymer composites. *Middle East J. Appl. Sci.* **5**, 1 (2015)
- Z. Xue, D. He, X. Xie, Poly(ethylene oxide)-based electrolytes for lithium ion batteries. *J. Mater. Chem. A* **3**, 19218 (2015)
- A. Sionkowska, Photochemical stability of collagen/poly(ethylene oxide) blends. *J. Photochem. Photobiol. A* **177**, 61 (2006)
- S. Ramesh, T.F. Yuen, C.J. Shen, Conductivity and FTIR studies on PEO-LiX [$\text{X}: \text{CF}_3\text{SO}_3^-$, SO_4^{2-}] polymer electrolytes. *Spectrochim. Acta A* **69**, 670 (2008)
- S. Ganesan, B. Muthuraaman, V. Mathew, M.K. Vadivel, P. Maruthamuthua, M. Ashokkumar, S.A. Suthanthiraraj, Influence of 2,6(N-pyrazolyl) isonicotinic acid on the photovoltaic properties of a dye-sensitized solar cell fabricated using poly(vinylidene fluoride) blended with poly(ethylene oxide) polymer electrolyte. *Electrochim. Acta* **56**, 8811 (2011)
- M.M.E. Jacob, S.R.S. Prabaharan, S. Radhakrishna, Effect of PEO addition on the electrolytic and thermal properties of PVDF- LiClO_4 polymer electrolytes. *Solid State Ionics* **104**, 267 (1997)
- H. Zhang, X. Xuan, J. Wang, H. Wang, Effect of poly(vinylidene fluoride) on solvation of NaSCN in PEO. *Spectrochim. Acta A* **61**, 347 (2005)
- L. Lee, S.-J. Park, S. Kim, Effect of nano-sized barium titanate addition on PEO/PVDF blend-based composite polymer electrolytes. *Solid State Ionics* **234**, 19 (2013)
- I.S. Elashmawi, N.H. Elsayed, R.A.S. Alatawi, PEO/PVDF nanocomposites preparation with functionalized single walled carbon nanotube. *Int. J. Nano Mater. Sci.* **4**, 24 (2015)
- L.H. Gaabour, Thermal spectroscopy and kinetic studies of PEO/PVDF loaded by carbon nanotubes. *J. Mater.* **2015**, 1 (2015)
- A.N. Ananth, S. Umopathy, J. Sophia, T. Mathavan, D. Mangalaraj, On the optical and thermal properties of in situ/ex situ reduced Ag NP's/PVA composites and its role as a simple SPR-based protein sensor. *Appl. Nanosci.* **1**, 87 (2011)
- M. Ghanipour, D. Dorrani, Effect of Ag-Nanoparticles Doped in Poly(vinyl Alcohol) on the Structural and Optical Properties of PVA Films. *J. Nanomater.* **2013**, 1 (2013)

23. A.k. Abbas, R.M. Naife, F.L. Rashid, A. Hashim, Optical properties of (PVA-PAA-Ag) nanocomposites. *Int. J. Sci. Res.* **4**, 2489 (2015)
24. S. Clémenson, L. David, E. Espuche, Structure and morphology of nanocomposite films prepared from polyvinyl alcohol and silver nitrate: influence of thermal treatment. *J. Polym. Sci. A* **45**, 2657 (2007)
25. H.M. Alhusiki-Alghamdi, N.S. Alghunaim, Spectroscopic studies of nanocomposites based on PEO/PVDF blend loaded by SWCNTs. *J. Mod. Phys.* **6**, 414 (2015)
26. T. Ohtake, Single phase $\text{Li}_4\text{Ti}_5\text{O}_{12}$ synthesis for nanoparticles by two steps sintering. *J. Mater. Sci. Chem. Eng.* **3**, 5 (2015)
27. T. Ohtake, K. Iijima, $\text{Li}_4\text{Ti}_5\text{O}_{12}$ synthesis with high specific surface area and single phase. *J. Mater. Sci. Chem. Eng.* **3**, 68 (2015)
28. C. Hong, A. Noviyanto, J. Ryu, J. Kim, D.Yoon, Effects of the starting materials and mechanochemical activation on the properties of solid-state reacted $\text{Li}_4\text{Ti}_5\text{O}_{12}$ for lithium ion batteries. *Ceram. Int.* **38**, 301 (2012)
29. Y. Wang, J. Wang, F. Wang, S. Li, J. Xiao, PVDF based all-organic composite with high dielectric constant. *Polym. Bull.* **60**, 647 (2008)
30. W. Ma, J. Zhang, S. Chen, X. Wang, Crystallization behavior and hydrophilicity of poly(vinylidene fluoride) (PVDF)/poly(styrene-co-acrylonitrile) (SAN) blends. *Colloid. Polym. Sci.* **286**, 1193 (2008)
31. M. Li, H.J. Wondergem, M.-J. Spijkman, K. Asadi, I. Katsouras, P.M. Blom, D.M. de Leeuw, Revisiting the δ -phase of poly(vinylidene fluoride) for solution-processed ferroelectric thin films. *Nat. Mater.* **12**, 433 (2013)
32. K.K. Kumar, M. Ravi, Y. Pavani, S. Bhavani, A.K. Sharma, V.V.R.N. Rao, Investigations on the effect of complexation of NaF salt with polymer blend (PEO/PVP) electrolytes on ionic conductivity and optical energy band gaps. *Physica B* **406**, 1706 (2011)
33. K.K. Kumar, M. Ravi, Y. Pavani, S. Bhavani, A.K. Sharma, V.V.R. NarasimhaRao, Investigations on PEO/PVP/NaBrcomplexed polymer blend electrolytes for electrochemical cell applications. *J. Membr. Sci.* **454**, 200 (2014)
34. V. Vetrivel, Dr.K. Rajendran, V. Kalaiselvi, Synthesis and characterization of pure titanium dioxide nanoparticles by sol-gel method. *Int. J. ChemTech Res.* **7**, 1090 (2015)
35. W. Liu, Y. Wang, X. Jia, B. Xia, The characterization of lithium titanate microspheres synthesized by a hydrothermal method. *J. Chem.* **2013**, 1 (2013)
36. M. Senna, M. Fabián, L. Kavan, M. Zúkalová, J. Briančin, E. Turianicová, P. Bottke, M. Wilkening, V. Šepelák, Electrochemical properties of spinel $\text{Li}_4\text{Ti}_5\text{O}_{12}$ nanoparticles prepared via a low-temperature solid route. *J. Solid State Electrochem.* **20**, 2673 (2016)
37. I.S. Elashmawi, N.H. Elsayed, F.A. Altalhi, The changes of spectroscopic, thermal and electrical properties of PVDF/PEO containing lithium nanoparticles. *J. Alloys Compd.* **617**, 877 (2014)
38. H. Bai, X. Wang, Y. Zhou, L. Zhang, Preparation and characterization of poly(vinylidene fluoride) composite membranes blended with nano-crystalline cellulose. *Prog. Nat. Sci.* **22**, 250 (2012)
39. N. Gondaliya, D.K. Kanchan, P. Sharma, P. Joge, Structural and conductivity studies of poly(Ethylene oxide) – silver triflate polymer electrolyte system. *Mater. Sci. Appl.* **2**, 1639 (2011)
40. S.M. Pawde, K. Deshmukh, Investigation of the structural, thermal, mechanical, and optical properties of poly(methyl methacrylate) and poly(vinylidene fluoride) blends. *J. Appl. Polym. Sci.* **114**, 2169 (2009)
41. I.S. Elashmawi, N.A. Hakeem, Effect of PMMA addition on characterization and morphology of PVDF. *Polym. Eng. Sci.* **48**, 895 (2008)
42. W.B. De Almedia, L.R.A. Costa, H.F. Dos Santos, M.C. Zerner, A theoretical investigation of the near UV and VIS electronic spectra for the fully deprotonated forms of anhydrotetracycline. *J. Chem. Soc. Perkin Trans.* **2**, 7, 1335 (1997)
43. B. Sharma, S.V. Bykov, S.A. Asher, UV resonance Raman Investigation of electronic transitions in α -helical and polyproline ii-like conformations. *J. Phys. Chem. B* **112**, 11762 (2008)
44. F.H. Abd El-kader, N.A. Hakeem, I.S. Elashmawi, A.M. Ismail, Structural, optical and thermal characterization of ZnO nanoparticles doped in PEO/PVA blend films. *Aust. J. Basic Appl. Sci.* **7**, 608 (2013)
45. F. Urbach, The Long-wavelength edge of photographic sensitivity and of the electronic absorption of solids. *Phys. Rev.* **92**, 1324 (1953)
46. J. Buckley, P. Cebe, D. Cherdack, J. Crawford, B.S. Ince, M. Jenkins, J. Pan, M. Reveley, N. Washington, N. Wolchover, Nanocomposites of poly(vinylidene fluoride) with organically modified silicate. *Polymer* **47**, 2411 (2006)
47. O.W. Guirguis, M.T.H. Moselhey, Thermal and structural studies of poly(vinyl alcohol) and hydroxypropyl cellulose blends. *Nat. Sci.* **4**, 57 (2012)